Origin of elemental carbon in snow from Western Siberia and northwestern European Russia during winter–spring 2014, 2015 and 2016

Nikolaos Evangeliou[1,*], Vladimir P. Shevchenko[2], Karl Espen Yttri[1], Sabine Eckhardt[1], Espen Sollum[1], Oleg S. Pokrovsky[3,4], Vasily O. Kobelev[5], Vladimir B. Korobov[2], Andrey A. Lobanov[5], Dina P. Starodymova[2], Sergey N. Vorobiev[6], Rona L. Thompson[1], Andreas Stohl[1]

[1] NILU - Norwegian Institute for Air Research, Department of Atmospheric and Climate Research (ATMOS), Kjeller, Norway.

[2] Shirshov Institute of Oceanology, Russian Academy of Sciences, Nakhimovsky prospect 36, 117997 Moscow, Russia.

[3] Geosciences Environment Toulouse, UMR 5563 CNRS, University of Toulouse, 14 Avenue Edouard Belin, 31400, Toulouse, France.

[4] N. Laverov Federal Center for Integrated Arctic Research, Russian Academy of Science, Sadovaya street, 3, 163000, Arkhangelsk, Russia.

[5] Arctic Research Center of the Yamalo-Nenets autonomous district, Vos'moy proezd, NZIA building, 629730, Nadym, Yamalo-Nenets autonomous district, Russia.

[6] BIO-GEO-CLIM Laboratory, Tomsk State University, 36 Prospect Lenina, 634050, Tomsk, Russia.

*Correspondence to: N. Evangeliou, NILU - Norwegian Institute for Air Research, Department of Atmospheric and Climate Research (ATMOS), Kjeller, Norway (Nikolaos.Evangeliou@nilu.no)

Abstract

Short–lived climate forcers have been proven important both for the climate and human health. In particular, black carbon (BC) is an important climate forcer both as an aerosol and when deposited on snow and ice surface, because of its strong light absorption. This paper presents measurements of elemental carbon (EC; a measurement-based definition of BC) in snow collected from Western Siberia and northwestern European Russia during 2014, 2015 and 2016. The Russian Arctic is of great interest to the scientific community due to the large uncertainty of emission sources there. We have determined the major contributing sources of BC in snow in Western Siberia and northwestern European Russia using a Lagrangian atmospheric transport model. For the first time, we use a recently developed feature that calculates deposition in backward (so-called retroplume) simulations allowing estimation of the specific locations of sources that contribute to the deposited mass.

EC concentrations in snow from Western Siberia and northwestern European Russia were highly variable depending on the sampling location. Modelled BC and measured EC were moderately correlated ($R = 0.53 - 0.83$) and a systematic region–specific model underestimation was found. Modelled underestimated observations by 42% (RMSE = 49 ng g^{-1}) in 2014, 48% (RMSE = 37 ng g^{-1}) in 2015 and 27% (RMSE = 43 ng g^{-1}) in 2016. For EC sampled in northwestern European Russia the underestimation by the model was smaller (fractional bias, FB > -100%). In this region, the major sources were transportation activities and domestic combustion in Finland. When sampling shifted to Western Siberia, the model underestimation was more significant (FB < -100%). There, the sources included emissions from gas flaring as a major contributor to snow BC. The accuracy of the model calculations was also evaluated using two independent datasets of BC measurements in snow covering the entire Arctic. The model underestimated BC concentrations in snow especially for samples collected in springtime.

1 Introduction

Black carbon (BC) is the strongest light-absorbing component of atmospheric aerosol and is formed by the incomplete combustion of fossil fuels, biofuels, and biomass (Bond et al., 2013). It is emitted directly into the atmosphere in the form of fine particles. BC is a major component of "soot", a complex light-absorbing mixture that also contains organic carbon (OC) (Bond et al., 2004). Combustion sources emitting BC include open biomass burning (forest, savanna, agricultural burning), residential biofuel combustion, diesel engines for transportation or industrial use, industrial processes and power generation, or residential coal combustion (Liu et al., 2011; Wang et al., 2011).

BC is important on a global perspective because of its impacts on human health and on climate. As a component of fine particulate matter (PM2.5), it is associated with negative health impacts, including premature mortality (Lelieveld et al., 2015; Turner et al., 2005). It absorbs solar radiation, has a significant impact on cloud formation and, when deposited on ice and snow, it accelerates ice melting (Hansen and Nazarenko, 2004). BC has a lifetime that can be as long as 9–16 days (Bond et al., 2013). After its emission, BC can travel over long distances (Forster et al., 2001; Stohl et al., 2006) and reach remote areas such as the Arctic. Arctic land areas are covered by snow in winter and spring, while the Arctic Ocean is partly covered by ice. Sea ice has a much higher albedo (≈0.5–0.7) compared to the surrounding ocean (≈0.06), thus presence of sea ice reduces the heat uptake of the ocean. Snow has an even higher albedo than sea ice and can reflect as much as 90% of the incoming solar radiation (Brandt et al., 2005; Singh and Haritashya, 2011). BC deposited on ice lowers its albedo, increases heat uptake by sea ice, accelerates its melting, and therefore decreases surface albedo both directly and indirectly.

Hegg et al. (2009) reported that snow in the Arctic often contains BC at concentrations between 1 and 30 ng g^{-1}, which can cause a snow albedo reduction of 1–3% in fresh snow and another 3–9% as snow ages and BC becomes more concentrated near the surface (Clarke and Noone, 1985). This solar radiation reflecting capacity of snow insulates the sea ice, maintains cold temperatures and delays ice melt in summertime. After the snow begins to melt and because shallow melt ponds have an albedo of approximately 0.2 to 0.4, the surface albedo drops to about 0.75 or even lower (0.15) as melt ponds grow and deepen (Singh and Haritashya, 2011). These changes have been found to be important for the global energy

balance (Flanner et al., 2007; Hansen and Nazarenko, 2004) and, if enhanced by BC, contribute to climate warming (Warren and Wiscombe, 1980).

Although BC in Arctic snow and ice has been found to be important for the Earth's climate (Flanner et al., 2007; Sand et al., 2015), its large-scale temporal and spatial distributions and exact origin are still poorly quantified (AMAP, 2015). Efforts to determine the concentrations of BC in snow across the Arctic were made by Clarke and Noone (1985), Doherty et al. (2010, 2013), Forsström et al. (2013), Ingvander et al. (2013) and McConnell et al. (2007). This paper presents measurements of Elemental Carbon (EC) concentrations in snow samples collected in spring 2014, 2015 and 2016 in the Kindo Peninsula (White Sea, Karelia), around Arkhangelsk in northwestern European Russia, and in Western Siberia. In the latter area, gas flaring emissions are very important. Flaring emissions are highly uncertain because both activity data and emission factors are largely lacking. According to the Global Gas Flaring Reduction Partnership (GGFR) (http://www.worldbank.org/en/programs/gasflaringreduction), nearly 50 billion m^3 of gas are flared in Russia annually. The Russian flaring emissions in the Nenets/Komi regions and in Khanty-Mansiysk are the major sources in Western Siberia and northwestern European Russia. It has been reported that gas flaring in Russia contributes about 42% to the annual average BC surface concentrations in the Arctic (Stohl et al., 2013).

The use of the terms EC and BC has been the topic of several scientific papers (for example, Andreae and Gelencsér, 2006; Bond et al., 2013; Petzold et al., 2013). Petzold et al. (2013) defined BC as a substance with 5 properties (see Table 1 in Petzold et al., 2013), for which no single measurement instrument exists that is sensitive to all of them at the same time. Consequently, BC cannot uniquely be measured, although some of its properties can, such as the absorption coefficient σ_{ap} and the elemental carbon (EC) concentration, both commonly measured in atmospheric monitoring networks across the world. Hence, the term BC should be used qualitatively.

In the present study, EC concentrations on ice from three campaigns measured with Thermal–Optical Analysis (TOA) (see section 2.2) are compared to simulation results from the Lagrangian particle dispersion model (LPDM) FLEXPART. The model is used here for the first time to quantify the sources contributing to BC in snow in Russia adopting a special feature that was developed recently.

2 Methodology

2.1 Collection and storage of snow samples

Fresh snow samples were collected along a north–south transect between Tomsk and the Yamal coast in February–March 2014 (23 samples, Table S 1), while in March 2015 sample collection took place in the Kindo Peninsula and near the port of Arkhangelsk in the White Sea (11 samples, Table S 1). Finally, in February–May 2016 samples were collected in the Kindo Peninsula, in Arkhangelsk and between Tomsk and Yamal (20 samples, Table S 1). These areas have been reported to receive pollution both from urban and gas flaring sources (Stohl et al., 2013). For example, the gas flaring sources located in Yamal and Khanty-Mansiysk (Russia) are in the main pathway along which sub-Arctic air masses travel to the Arctic (Stohl et al., 2006). All sampling points were located more than 500 m away from roads to minimize the direct influence from local traffic emissions. Information about sample collection such as the location of sampling, the amount of snow collected and the depth at which snow was sampled is reported in Table S 1 and the sample locations are plotted in Figure 1.

Sampling was performed using a metal-free technique using pre-cleaned plastic shovels and single–use vinyl gloves. Samples were stored in polyethylene bags which had been thoroughly washed with 1 M HCl and rinsed with abundant deionised ultrapure water in the laboratory prior to their use. After returning the samples to the laboratory, the snow was allowed to melt at ambient temperature (18–20°C), and immediately filtered through quartz 47 mm fibre filters (2500QAT-UP Pall for samples collected in 2014 and QM-A Whatman for samples collected in 2015 and 2016). The filters were dried at 60–70°C, wrapped in aluminum foil and stored in a refrigerator. Quartz fiber filter collection efficiency of BC in liquid samples can be less than 100% (Hadley et al., 2010; Ogren et al., 1983). To what extent this has affected the levels reported in the present study is unknown. Thus the results presented should be regarded as conservative estimates based on the assumption that some BC might have been lost during filtration.

2.2 Elemental Carbon measurements by Thermal–Optical Analysis (TOA)

Elemental carbon (EC) content of the filters was measured at NILU's laboratories by thermal-optical analysis (TOA), using the Sunset laboratory OC/EC instrument operated according to the EUSAAR-2 protocol (Cavalli et al., 2010). A 1.5 cm^2 punch was cut from the filtered snow samples for the analysis. Transmission was used for organic carbon (OC) charring

correction. Performance of the OC/EC instrument's is regularly intercompared as part of the joint European Monitoring and Evaluation Programme (EMEP) Aerosols, Clouds, and Trace gases Research InfraStructure Network (ACTRIS) quality assurance and quality control effort (Cavalli et al., 2015).

2.3 Measurements of carbonate (CO_3^{2-})–carbon by Thermal–Optical Analysis (TOA) following thermal-oxidative pre-treatment

The content of carbonate (CO_3^{2-})–carbon on the filters was measured by TOA, following thermal-oxidative pretreatment based on the approach described by Jankowski et al. (2008). A punch of 1.5 cm^2 from each filter was heated at 450 °C for 2 hours in ambient air to remove OC and EC, but not CO_3^{2-}–carbon. The filter punch was subjected to TOA immediately (30 sec) after thermal-oxidative pre-treatment. The split time (between OC and EC) obtained for each filter punch used to determine the filter samples' content of EC (section 2.2) was also used to apportion CO_3^{2-}–carbon to OC and/or EC. The influence of CO_3^{2-}–carbon evolving as EC, was accounted for by the following equation:

$$EC_{CO_3^{2-}}^{corr} = EC - EC_{CO_3^{2-}}$$

where $EC_{CO_3^{2-}}^{corr}$ is elemental carbon corrected for CO_3^{2-}–carbon that evolved as EC during TOA, EC is elemental carbon and $EC_{CO_3^{2-}}$ is CO_3^{2-}–carbon that evolved as EC during TOA. Applying this correction, EC values were 5-22% lower (see Supplementary Information).

2.4 Emissions and modelling of black carbon

The concentrations of BC in snow were simulated with the LPDM FLEXPART version 10 (Stohl et al., 1998, 2005). The model was driven with operational meteorological wind fields retrieved from the European Centre for Medium-Range Weather Forecasts (ECMWF) of 3–hour (for the years 2014 and 2015) and hour (for the year 2016) temporal resolution. The ECMWF data have 137 vertical levels and a horizontal resolution of 1°×1° for the 2014 and 2015 simulations and 0.5°×0.5° for the 2016.

The simulations were conducted in backwards time ("retroplume") mode, using a new feature of FLEXPART to reconstruct wet and dry deposition with backward simulations (Eckhardt et al., 2017). This new feature is an extension of the traditional possibility to simulate atmospheric concentrations backward in time (Seibert and Frank, 2004; Stohl et al., 2003). It is computationally efficient because it requires only two single tracer transport

simulations (one for wet deposition, one for dry deposition) for each measurement sample. To reconstruct wet deposition amounts of BC, computational particles were released at altitudes of 0 to 20 km at the locations where snow samples were taken, whereas to reconstruct dry deposition, particles were released between the surface and 30 m at these locations. All released particles represent a unity deposition amount, which was converted immediately (i.e., upon release of a particle) to atmospheric concentrations using the deposition intensity as characterized either by dry deposition velocity or scavenging rate (for further details, see Eckhardt et al., 2017). The concentrations were subsequently treated as in normal "concentration mode" backward tracking (Seibert and Frank, 2004) to establish source-receptor relationships between the emissions and deposition amounts. The termination time of the particle release was the time at which the snow sample was collected, whereas the beginning time was set as the time when the ECMWF precipitation at the sampling site, accumulated backward in time, was equal to the water equivalent of the snow sample, up to the specified sampling depth.

The model output consists of a spatially gridded sensitivity of the BC deposition at the sampling location (receptor) to the BC emissions, equivalent to the backwards time mode output for concentrations (Seibert and Frank, 2004; Stohl et al., 2003). BC deposition at the snow sampling point can be computed (in mass per unit area) by multiplying the emission sensitivity in the lowest model layer (the footprint emission sensitivity) with gridded emissions from a BC emission inventory and integrating over the grid. The deposited BC can be easily converted to BC snow concentration by taking into account the water equivalent depth of the snow from ECMWF (in mm). In the present study, the ECLIPSE (Evaluating the CLimate and Air Quality ImPacts of ShortlivEd Pollutants) version 5 emission inventory (Klimont et al., 2016; Stohl et al., 2015) was used (http://www.iiasa.ac.at/web/home/research/researchPrograms/air/Global_emissions.html). The total emissions of BC from ECLIPSE in the areas of study are shown in Figure 1 (left panel).

BC was assumed to have a density of 2 g m^{-3} in our simulations and a logarithmic size distribution with an aerodynamic mean diameter of 0.25 μm and a logarithmic standard deviation of 0.3. Each computational particle released in FLEXPART represents an aerosol population with a lognormal size distribution (see Stohl et al., 2005). Assumed aerodynamic mean diameter and logarithmic standard deviation are used by FLEXPART's dry deposition scheme, which is based on the resistance analogy (Slinn 1982), and they are consistent with

209 those used in other transport models (see Evangeliou et al., 2016; Shiraiwa et al., 2008).
210 Below-cloud scavenging was determined based on the precipitation rate taken from ECMWF.
211 The in-cloud scavenging was based on cloud liquid water and ice content, precipitation rate
212 and cloud depth from ECMWF (Grythe et al., 2017). The FLEXPART user manual (available
213 from http://www.flexpart.eu) provides more information. All modelling results for this
214 sampling campaign can be viewed interactively at the URL
215 http://niflheim.nilu.no/NikolaosPY/SnowBC_141516.py.

216 ## 3 Results

217 In this section the main results of EC concentrations in snow are presented, in contrast
218 to simulated BC concentrations with FLEXPART. The statistical dependence of the datasets
219 is assessed using the Pearson product-moment correlation coefficient. For further validation,
220 the fractional bias (FB) of each individual sample was calculated together with the mean
221 fractional bias (MFB) for observed and modelled concentrations as follows:

$$FB = \frac{C_m - C_o}{(C_m + C_o)/2} \times 100\% \;\; and \;\; MFB = \frac{1}{N}\sum_{i=1}^{N} \frac{C_m - C_o}{(C_m + C_o)/2} \times 100\%$$

222 where C_m and C_o are the modelled BC and measured EC concentrations and N is the total
223 number of observations for each year. FB is a useful model performance indicator because it
224 is symmetric and gives equal weight to underestimations and overestimations (it takes values
225 between -200% and 200%). It is used here to show the locations where modelled BC
226 concentrations in snow over- or underestimate observations. Finally, for the same reasons, the
227 root mean square error (RMSE) was also computed, which is frequently used to measure
228 differences between values predicted by a model and the values actually observed (see Figure
229 S 1 – S 3).

230 ### 3.1 Elemental Carbon concentrations measured in snow

231 The spatial distribution of EC measured in snow samples from northwestern European
232 Russia and Western Siberia is shown in Figure 1(c) for each of the campaigns (2014, 2015
233 and 2016) and are also summarised in Table S 2. There was large spatial variability in the
234 distribution of EC in snow in 2014 ranging from 3 to 219 ng g^{-1}, with a median (±interquartile
235 range) of 23±49 ng g^{-1}. The highest EC concentrations in 2014 were observed in Western
236 Siberia near Tomsk (147 to 219 ng g^{-1}). FLEXPART emission sensitivities for these samples

showed that the air was coming from the north and the east (see in http://niflheim.nilu.no/NikolaosPY/SnowBC_141516.py). This explains the high concentrations of EC, as most of the anthropogenic BC sources are located in these regions. In the rest of the snow samples for 2014, EC concentrations between 4 and 170 ng g^{-1} were observed. High concentrations were observed near the Ob River coinciding with air masses arriving mainly from Europe. During the 2015 field campaign, EC concentrations were the highest near Arkhangelsk (175 ng g^{-1}), for which FLEXPART showed that the air was coming from nearby areas (http://niflheim.nilu.no/NikolaosPY/SnowBC_141516.py). Therefore, it is likely that the samples were affected by direct emissions from the city or the port of Arkhangelsk. During the same campaign, snow samples collected in the Kindo peninsula (on the White Sea coast) showed high variability in EC concentrations (range: 46 – 152 ng g^{-1}, median=70±34 ng g^{-1}). According to FLEXPART emission sensitivities, air masses were transported to Kindo peninsula from central and southern Europe driven by an anticyclone over Scandinavia (http://niflheim.nilu.no/NikolaosPY/SnowBC_141516.py). Finally, for the snow samples collected outside Arkhangelsk, at the Kindo peninsula, and close to the Yamal Peninsula in Western Siberia in 2016, EC concentrations ranged between 7–161 ng g^{-1} (median: 40±47 ng g^{-1}). Outside Arkhangelsk, EC concentrations varied widely from 31 to 161 ng g^{-1} with a median concentration in this region of 61±43 ng g^{-1}. This is far below the 175 ng g^{-1} observed in 2015, although there was only one sample collected in that year. In the Kindo Peninsula, EC was relatively constant in 2016 ranging between 25 and 35 ng g^{-1} (median = 28±4 ng g^{-1}), which is more than 60% lower compared with the 2015 values (median = 70±34 ng g^{-1}). Finally, between Tomsk and Yamal, EC concentration was highly variable (7 – 119 ng g^{-1}) due to the different EC sources affecting snow (median = 50±34 ng g^{-1}). For instance, it is expected that gas flaring affects snow close to Yamal, while snow collected in the south (Tomsk) is likely influenced by sources in Europe or local urban emissions. Nevertheless, the highest concentrations (>100 ng g^{-1}) were observed north of 68°N, in the Yamal Peninsula.

We compared the measured EC concentrations in the snow samples with those calculated by FLEXPART. For this, the emission sensitivities were multiplied with the total emission fluxes from ECLIPSE (section 2.4). A scatter plot of modelled and measured snow concentrations is presented in Figure 1 (b). The results show a good correlation between modelled BC and measured EC concentrations for the 2015 and 2016 campaigns ($R_{2015} = 0.83$ and $R_{2016} = 0.68$, $p - value < 0.05$), but weaker correlation for 2014 ($R_{2014} = 0.53$,

$p - value < 0.05$). The FB for individual samples is shown in Figure S 1. The MFB of the model for the 2014 snow measurements was –42%, which shows that the model underestimated observations. In total, the model underestimated concentrations by 30% – 168% for 17 out of 23 samples, whereas for the rest (six samples) FB values ranged between 20% and 148% (median MFB: –56%±72%) (Figure S 1). In 2015, the model underestimated observations by 48% (median MFB: –56%±29%) for 11 out of 12 samples (FB between –101% and –7%, while one value was found to be 12%). For 2016, FB values of the simulated concentrations of BC in snow showed another set of underestimation (median: –13%±60%) between 0.3% and 198% for 12 out of 19 samples. For the remaining seven samples, the model predicted higher concentrations compared with observations (10% to 75%) (Figure S 1). RMSE values were estimated to be quite high, between 37 and 49 ng g^{-1}, due to the large variation of the observed EC concentrations.

The levels of EC in snow presented here are relatively high compared to previously reported concentrations in the Arctic. Apart from Aamaas et al. (2011) who measured maximum EC concentration in snow close to the airport of Svalbard of more than 1000 ng g^{-1}, most of the reported levels of EC in the relevant literature are close to our findings. For instance, Ruppel et al. (2014) found that EC concentrations have been increasing up to 103 ng g^{-1} since 1970 in Svalbard. McConnell et al. (2007) reported that the BC concentrations measured at the D4 ice-core site in Greenland were 10 ng g^{-1}, at maximum, which most likely originated from biomass burning in the conifer–rich boreal forest of the Eastern and Northern United States and Canada. Forsström et al. (2013) reported concentrations as high as 88 ng g^{-1} in Scandinavia, and lower ones at higher latitudes (11–14 ng g^{-1} in Svalbard, 7–42 ng g^{-1} in the Fram Strait, and 9 ng g^{-1} in Barrow). Svensson et al. (2013) collected snow samples from Tyresta National Park and Pallas-Yllästunturi National Park in Sweden. Tyresta is a relatively polluted site located circa 25 km from the city centre of Stockholm with a population of about 2 million people. Yllästunturi National Park is located in Arctic Finland and a clean site with no major city influencing the local and regional air. The concentration of EC in Pallas-Yllästunturi was between 0 and 140 ng g^{-1}, while in Tyresta the BC concentrations were up to more than 7 times higher (53–810 ng g^{-1}). Furthermore, Doherty et al. (2010) in the most complete dataset for the Arctic snow and ice BC reported highly variable concentrations (up to 800 ng g^{-1}) for five consecutive years (2005–2009). Finally, in the most recent dataset for snow BC, Macdonald et al. (2017) reported BC concentrations ranging from 0.3 to 15 ng g^{-1} were reported for the samples collected near the Alert observatory (see section 4.1).

3.2 Sources and origin of BC

We further analysed the model output in order to calculate relevant contributions from various BC source types to BC concentrations in snow (for method description, see section 2.4). ECLIPSE emissions include waste burning (WST), industrial combustion and processing (IND), surface transportation (TRA), power plants, energy conversion, and extraction (ENE), residential and commercial combustion (DOM), gas flaring (FLR), while biomass burning (BB) emissions were adopted from the Global Fire Emissions Database, Version 4 (GFEDv4.1) (Giglio et al., 2013). The results are depicted in Figure 2 for the sampling campaigns of 2014, 2015 and 2016 in Western Siberia and North-Western European Russia, sorted from the northernmost to the southernmost sampling location.

In 2014, TRA contributed about 18%, on average, to the simulated BC in snow, DOM 28%, FLR 44%, whereas ENE and IND were less significant. Maxima of TRA, DOM, and FLR contributions were observed at a latitude of about 65°N, where measured EC and modelled BC were similar. An example of the contribution from the aforementioned dominant sources to snow BC concentrations for the highest measured EC concentration in snow is shown in Figure 3. The transport sector includes emissions from all land-based transport of goods, animals and persons. It is more significant in southern Russia and close to the borders with Kazakhstan and Mongolia, where a large number of major Russian cities (e.g., Moscow, Kazan, Samara, Yekaterinburg, Tomsk, Novosibirsk, Krasnoyarsk, etc…) are located and connected with each other by federal highways. Residential and commercial combustion includes emissions from combustion in households and public and commercial buildings. Therefore, it is expected to be high for areas that consist of large population centres (Figure 3). FLR emissions were found to contribute the most in this example with a total concentration from this sector of 19.7 ng g^{-1} (compared with 12.6 and 16.5 ng g^{-1} in TRA and DOM, respectively) (Figure 3).

In the Kindo Peninsula and in Arkhangelsk, where snow sampling took place in 2015, the main contributions to snow BC were from DOM (47%), TRA (30%), BB (7%), and FLR (6%) (see Figure 2). Similar to EC measurements in snow, simulated BC was also higher than in 2014, as the sampling sites were located closer to strong sources in Europe (Kindo) and close to a populated area (Arkhangelsk) with a strong regional impact. The highest concentration of EC was observed in the Kindo Peninsula (33.13°E – 66.53°N). Figure 4 shows the spatial distribution of emissions that contributed to simulated snow BC at the

sampling point where the highest BC concentration was observed. In this case, TRA and DOM emissions from Europe mostly affected snow in the Kindo Peninsula whereas FLR emissions were very low due to the long distance from the sampling point. Emissions from an unusual late winter/early spring episode of BB in the borders of Belarus, Ukraine and Russia also affected BC concentrations in snow in northwestern European Russia (Figure 4). The importance of episodic BB releases in Russia, the miscalculation of satellite retrieved BB emissions and their impact in Arctic concentrations in early spring has been explained by Evangeliou et al. (2016) and Hao et al. (2016). BB emissions, originating mostly from Eastern Europe, contributed about 19.4 ng g^{-1} to the snow concentration at the receptor point (Figure 4). TRA and DOM emissions were the dominant sources for this sampling point, contributing 33.6 and 47.2 ng g^{-1}, respectively (Figure 4).

Finally, in 2016, when samples were collected at the Kindo Peninsula, in Arkhangelsk and in Yamal, DOM, FLR and TRA contributed, on average, 31%, 29% and 27%, respectively (see Figure 2 (c)). Similar to the measured EC concentrations in snow, simulated concentrations of BC in 2016 were lower than those in 2015, on average. The highest measured EC concentration was observed in the Khanty-Mansiysk region (72.94°E – 65.36°N), which mirrors the simulated BC concentration at the same point very well. The much higher contribution from TRA at this sampling point (38.6 ng g^{-1}) (Figure 5 (b)) is attributed to emissions from Southern Russia (e.g., Tomsk), where all the main cities in Russia are located. Another large fraction of TRA emissions comes from Central and Eastern Europe (see also in http://niflheim.nilu.no/NikolaosPY/SnowBC_141516.py). Similar to TRA, emissions from DOM were mostly transported to Khanty-Masiysk from Central and Eastern Europe, as well as from Turkey contributing 36.6 ng g^{-1} (Figure 5). As previously mentioned, the sampling point where the highest EC concentration was measured is located inside the largest gas flaring region of Russia. In addition, the corresponding emission sensitivity maps showed that the air was coming from south passing directly through this high emission region making FLR emissions the highest contributing source (88.8 ng g^{-1}) (Figure 5).

4 Discussion

4.1 Cross validation of modelled BC concentrations with public datasets

In this section, we present an effort to further validate our model calculations of BC concentrations in snow. For this purpose, BC concentrations in snow that were adopted from

Doherty et al. (2010) were compared with modelled BC concentrations in snow that were simulated with FLEXPART as described in section 2.4. Samples were collected in Alaska, Canada, Greenland, Svalbard, Norway, Russia, and the Arctic Ocean during 2005–2009, on tundra, glaciers, ice caps, sea ice, frozen lakes, and in boreal forests. Snow was collected mostly in spring, when the combination of snow cover and exposure to sunlight is at maximum and before the snow had started to melt. Samples of melting snow collected in the summer of 2008 from Greenland and from Tromsø, Norway, were removed from the study, as we have no knowledge about the depth of the melt layer and effects of the percolation of meltwater through the snowpack. All samples were collected away from local sources of pollution. In many locations (Canadian Arctic, Russia, Greenland, Tromsø and Ny-Ålesund) samples were gathered at different depths throughout the snowpack, giving information on the seasonal evolution of BC concentrations as the snow accumulated (and/or sublimated) throughout the winter. In these cases only the surface BC was taken into account. The snow was melted and filtered, and the filters were analysed in a specially designed spectrophotometer system to infer the concentration of BC (for more information see Doherty et al., 2010). In contrast to our findings for the origin of snow BC in the Russian Arctic, a source apportionment analysis perform in the 2008 and 2009 measurements (Hegg et al., 2010) from this dataset showed that the dominant source of BC in the Arctic snow pack was biomass burning. Specifically in Eastern Siberia biomass burning of crops and grasslands contributed more snow BC in high latitudes than boreal forest fires, in contrast to the Canadian Arctic.

A comparison of modelled (FLEXPART) and measured BC concentrations (Doherty et al., 2010) in snow is depicted in Figure S 2. The model captures snow BC concentrations relatively well in most of the Arctic regions except for the Canadian Arctic, where the modelled concentrations of snow in 2007 were significantly higher. Samples from the same region in other years showed moderate agreement with modelled values. Similar to our finding for the new Russian measurements, the model underestimated deposition by 51%. The RMSE was estimated to be 52 ng g^{-1}, which is acceptable considering that the variation of snow concentrations in the dataset ranged from 0.3 to 783 ng g^{-1}. The highest measured concentrations of snow BC were observed in Russia, where the model showed a good spatial agreement. For instance, the highest values were obtained in Western Siberia, close to the gas flaring regions of the Nenets/Komi oblast, as well as in southeastern and northeastern Russia, where air masses were arriving from high emitting sources in southeastern Asia. Lower biases

400 in modelled BC concentrations were observed in northern Siberia with the exception of a few
401 samples at the coasts of the Kara Sea and northeastern Siberia. Furthermore, biased BC
402 concentrations were also observed in Greenland and northern Canada. In Western Siberia, BC
403 in snow presented in Doherty et al. (2010) between 2005–2009 was 80±63 ng g^{-1} on average,
404 which is very close to the average value of measured EC obtained from the sampling 2014–
405 2016 campaigns (50±46 ng g^{-1}).

406 From total number of samples presented in (Doherty et al., 2010) that were used here
407 for validation, only six were collected in the Yamal Peninsula similar as part of the data
408 presented in the current paper. The rest was collected in Nenets/Komi region and in Eastern
409 Russia and cannot be directly compared with snow EC measurements from the 2014 – 2016
410 campaigns. BC concentrations in Yamal Peninsula in 2007 ranged from 4.1 to 17.6 ng g^{-1}
411 (median±interquartile: 10.3±4.9 ng g^{-1}). In the same region, we report EC concentrations to be
412 more than double varying between 6.6 to 55 ng g^{-1} (median±interquartile: 27.8±25.5 ng g^{-1}),
413 whereas there were two samples that showed EC concentrations of more than 100 ng g^{-1}. As
414 mentioned in section 2.1 the sampling of snow for the EC analysis took place more than 500
415 m away from roads to minimize influence from traffic emissions, while a similar statement is
416 also found in the Doherty et al. (2010) data. It is not clear whether the observed discrepancy
417 arises as a measurement artefact (even though every effort has been taken in both papers to
418 follow a robust protocol) or from real spatio-temporal variation.

419 Modelled BC concentrations simulated with FLEXPART were also compared with
420 snow BC concentrations from samples collected at the Global Atmosphere Watch
421 Observatory at Alert, Nunavut, from September 14th, 2014 to June 1st, 2015 and they are
422 available in Macdonald et al. (2016). Alert is a remote outpost in the Canadian high Arctic, at
423 the northern coast of Ellesmere Island (82°27' N, 62°30' W), with a small transient
424 population of research and military personnel. Sampling details and analytical methodologies
425 used for the analysis of BC can be found in Macdonald et al. (2016). BC concentrations in
426 FLEXPART were simulated as in all previous analyses described in this paper (see section
427 2.4.). Timeseries of simulated and measured BC are depicted in Figure S 3 for the whole
428 sampling period. As before, a correlation coefficient (R) of 0.63 indicates that our model
429 captures the temporal variation of the measured BC in snow. The RMSE was estimated to be
430 almost 63 ng g^{-1}, a relatively high value. The MFB of 47% indicates a strong overestimation
431 of snow concentrations, although in many samples the opposite was also observed (Figure S

3). This is in contrast to the previous data sets discussed, for which the model underestimated measurements.

Further analysis was carried out to adequately understand the origin of the aforementioned overestimations in the Canadian Arctic in both datasets (Doherty et al., 2010; Macdonald et al., 2017), as they are shown to be rather systematic. For this reason, we have calculated the average footprint emission sensitivities and the average BC contribution from the major sources in ECLIPSE for the 2007 snow samples in the Canada Arctic and for Alert samples. We have chosen these samples, because they were three or more times higher than the observations and in this way we can locate the observed overestimations predicted with FLEXPART (Figure 6).

Regarding the model overestimation for the 2007 samples, the average footprint emission sensitivity showed that the air was coming from continental regions of Canada with a smaller contribution from Scandinavia (Figure 6). The highest emission sources for these samples were TRA and DOM that contributed almost 80% to the snow concentrations, whereas forest fires were less important at the time of sampling. Two hot spots were identified, one along the borders of Canada with USA and another, of smaller intensity, in southeastern Asia. A similar emission sensitivity was obtained for the same area of the Canadian Arctic in 2009 only slightly shifted to the north; simulated concentrations were in very good agreement with observations (Figure S 2). This shows that the model overestimation for the 2007 samples is likely attributed to an overestimation of TRA and DOM sources in North America in ECLIPSE for 2007. For the Alert samples, for which the model strongly overestimated BC, the major sources were TRA and FLR, which contributed 55%, and BB which contributed about 7 ng g^{-1} (22%) on average (Figure 6). Anthropogenic BC arriving from Europe and Russia has been previously shown to be important for Alert air pollutant concentrations (Sharma et al., 2013). The model overestimation of BC in snow samples at Alert needs further investigation. It is likely that it originates from anthropogenic emissions in northwestern America or in Europe, because forest fires in Canada and Russia, although important for Alert (e.g., Qi et al., 2017), were not significant in the present comparison.

4.2 Model deviation from snow EC measurements and region–specific contribution of sources

It has been shown that measured concentrations of EC in snow in northwestern European Russia and Western Siberia were underestimated in FLEXPART (Figure 2). This was confirmed by the calculated fractional bias (see section 3.2), the spatial distribution of which is shown in Figure S 1. To examine whether this underestimation was due to missing emission sources or errors in modelled transport and deposition, we have calculated the average footprint emission sensitivity for those sampling points, for which FLEXPART strongly ($FB < -100\%$) and slightly ($-100\% < FB < 0\%$) underestimated the observed values. The average footprint emission sensitivities are shown in Figure 7 together with the locations of active fires in the last two months before the sample collection. The fire data were adopted from MODIS (Moderate Resolution Imaging Spectroradiometer) (Giglio et al., 2003) and the gas flaring facilities from the Global Gas Flaring Reduction Partnership (GGFR) (http://www.worldbank.org/en/programs/gasflaringreduction).

When the model strongly underestimated the measured EC ($FB < -100\%$), the average footprint emission sensitivity showed the highest values over the Yamal Peninsula and the agglomeration of many gas flares in Khanty-Mansiysk (Figure 7 (b)). This might confirm the finding of Huang et al. (2014) that gas flaring emissions in the ECLIPSE inventory, while very high, are still underestimated. According to a related study by Huang and Fu (2016), Russia contributes 57% to the global BC emissions from gas flaring. Underestimation of modelled atmospheric concentrations compared to observations from the Barents and Kara Seas was recently also reported by Popovicheva et al. (2017), although the underestimation was relatively small.

When FLEXPART showed a moderate underestimation of EC concentrations in snow ($-100\% < FB < 0\%$), the emission sensitivity was high near Arkhangelsk and over Scandinavia (Figure 7). BC emissions in Scandinavia are considered relatively low in most inventories and contribute no more than 6.5% to the global emissions in ACCMIP (Aerosol Chemistry Climate Model Intercomparison Project) (Lamarque et al., 2013), 6.2% in EDGARv4.2 (Emission Database for Global Atmospheric Research) (Olivier et al., 2005), 2.1% in MACCity (Monitoring Atmospheric Composition & Climate / megaCITY - Zoom for the ENvironment) (Hollingsworth et al., 2008; Stein et al., 2012) and 3.3% in ECLIPSE (Klimont et al., 2016). The highest emission sensitivity was found over northwestern Russia (Figure 7), a region which includes Murmansk. Pollution levels in Murmansk could be high due to emissions from local industry, mining, heating and transport (Law and Stohl, 2007).

Another potential source region was Nenets/Komi area and Western Kazakhstan, where a few other flaring facilities are located (Figure 7).

Figure 7 shows that the underestimation of observed EC concentrations in snow strongly depends on the region, where samples are collected. In Western Siberia, the underestimation was larger than in northwestern European Russia. For this reason, we have computed the average region–specific emission sensitivities and the average region–specific contribution from the major polluting sources identified in ECLIPSE dataset. We distinguish between three regions, northwestern European Russia, Western Siberia (north of 62 °N) and Western Siberia (south of 62 °N) (Figure S 4 – S 6). For the samples collected in northwestern European Russia (Figure S 4), an average contribution of 21.6 ng g^{-1} from all sources was estimated to have originated mainly from TRA (7.7 ng g^{-1}) and DOM (10.4 ng g^{-1}) sources in Finland. The contribution from BB and FLR emissions was insignificant (8% and 6%, respectively), whereas the rest of the ECLIPSE sources were negligible (IND, ENE, WST). For the samples collected at high latitudes in Western Siberia, the average contribution from all sources was more than 4 times higher (86 ng g^{-1}) than those observed in northwestern European Russia (Figure S 5). FLR emissions accounted for 40% of the total contribution, which reflect the proximity of the sampling site to the main flaring facilities of Russia. The average contribution from TRA activities in Europe and southeastern Russia to the northern part of Western Siberia was 24%. Finally, DOM emissions in Eastern Europe also contributed another 28%. Finally, for the samples that were collected in the southern part of the Western Siberia an average contribution of 47.4 ng g^{-1} was estimated from all sources included in ECLIPSE (Figure S 6). The highest contributing categories were TRA and DOM, whereas FLR appeared to contribute less, although the sampling site is close to Khanty-Mansiysk flaring region. This is attributed to the prevailing winds that forced flaring emissions to a northernmost direction opposite to the location of the sampling stations (see Figure S 6).

Overall, the region–specific analysis of the sources contributing to modelled BC in snow showed that the DOM, FLR and/or TRA sources might explain the model underestimation in high Arctic. However, in the most recent assessments of BC of the higher Arctic (Popovicheva et al., 2017; Winiger et al., 2017), it was shown that ECLIPSE captures levels of BC quite well, whereas FLR emissions might have a smaller impact in the Central Siberian Arctic (Tiksi) than previously estimated. Surprisingly, the average contribution from BB in lower latitudes was extremely low in all Western Siberia (Figure S 5 and S 6), despite the fact that sampling took place in springtime, where BB becomes important. Evangeliou et

al. (2016) reported that using a different dataset, that is based on the same approach as GFED, but includes updated emission factors for Eurasia, surface concentrations of BC in the Arctic stations can be substantially higher. This shows the need for further investigation of BC sources in the Russian Arctic.

5 Conclusions

We have analysed snow samples collected in Western Siberia and northwestern European Russia in 2014, 2015 and 2016 with respect to EC. This region is of major interest due to its large uncertainty in BC emissions and because it is located in the main transport route of BC to the Arctic. An effort to constrain the sources that contribute to measured concentration in BC in snow was made using the LPDM FLEXPART (version 10).

The observed EC levels in snow varied widely within and between regions (3–219 ng g^{-1} for 2014, 46–175 ng g^{-1} in 2015 and 7–161 ng g^{-1} in 2016), and are in the upper range of previously reported concentrations of EC and BC in snow in the Arctic region. However, the observed levels presented here appear typical for Western Siberia, which is subject to high domestic Russian emissions as well as to transport from distant European ones.

The snow BC concentrations predicted by the model are in a fair agreement with EC observations over Western Siberia and northwestern European Russia ($R = 0.5 - 0.8$). However, the calculated negative MFB values (-48% to -27%) showed that the model systematically underestimated observations in Russia. This underestimation strongly depended on the region where the samples were collected. In northwestern European Russia, the main contributing sources were TRA and DOM mainly from adjacent regions in Finland. TRA and DOM contributed double to snow BC sampled at low latitudes of Western Siberia (<60°N) as compared to samples collected over regions above 60°N; the majority of these emissions originating from highly populated centres in Central Europe. Finally, in higher latitudes of Western Siberia (>60°N), snow BC concentrations were further increased mainly due to FLR emissions from facilities located close to the snow sampling points.

The modelled BC concentrations in snow were further investigated using two independent public measurement datasets that include samples from all over the Arctic for the period 2005 to 2009 and from Alert in 2014 and 2015. The model captured levels of BC fairly well despite the large variation in measured concentrations. An exception was observed in North America in spring 2007 and in Alert observatory in late winter – early spring 2015. In

both cases, the major sources were along the Canadian borders with USA and in Western Europe. Considering the fact that similar deviations were not observed in samples collected in the area during other years, it is likely that some of the prevailing sources of BC in this region show strong temporal variability in their emissions, and this is not taken into account in ECLIPSE inventory. Previously reported average measurements of BC concentrations in snow in Western Siberia and northwestern European Russia were 80±43 ng g^{-1}, which is about 30% higher than the EC measurements presented here (50±46 ng g^{-1}).

Data availability. All data used for the present publication can be obtained from the corresponding author upon request.

Competing interests. The authors declare that they have no conflict of interest.

Acknowledgements. We would like to acknowledge the project entitled "Emissions of Short-Lived Climate Forcers near and in the Arctic (SLICFONIA)", which was funded by the NORRUSS research program of the Research Council of Norway (Project ID: 233642) and the Russian Fund for Basic Research (project No. 15-05-08374) for funding snow sampling in the White Sea catchment area. We also thank Sergey Belorukov, Andrey Boev, Anton Bulokhov, Victor Drozdov, Sergey Kirpotin, Ivan Kritzkov, Rinat Manasypov, Ivan Semenyuk, and Alexander Yakovlev for helping during the three expeditions and Academician Alexander P. Lisitzin for his valuable recommendations. O. S. Pokrovsky and S. N. Vorobiev acknowledge support from BIO-GEO-CLIM grant No 14.B25.31.0001 for sampling in Western Siberia. Acknowledgements are also owed to IIASA (especially Chris Heyes and Zig Klimont) for providing the BC emission dataset. Computational and storage resources for the FLEXPART simulations have been provided by NOTUR (NN9419K) and NORSTORE (NS9419K). All plots from FLEXPART simulations have been included in an interactive website for fast visualization (http://niflheim.nilu.no/NikolaosPY/SnowBC_141516.py). All results can be accessed upon request to the corresponding author of this manuscript.

Author Contributions. N. Evangeliou designed and performed the modelling experiments and wrote the paper. V. P. Shevchenko organised and performed the sampling of EC, K.-E. Yttri performed all the TOA of the snow samples. S. Eckhardt modified FLEXPART model for the calculation of footprint emission sensitivities for deposited mass. E. Sollum wrote an algorithm that computes the starting date of the FLEXPART releases based on the water equivalent volume from ECMWF. O. S. Pokrovsky, V. O. Kobelev, V. B. Korobov, A. A.

Lobanov, D. P. Starodymova and S. N. Vorobiev assisted the sampling campaigns in Western Siberia and northwestern European Russia during 2014–2016. R. L. Thompson and A. Stohl supervised the study and wrote parts of the paper.

References

Aamaas, B., Bøggild, C. E., Stordal, F., Berntsen, T., Holmén, K. and Ström, J.: Elemental carbon deposition to Svalbard snow from Norwegian settlements and long-range transport, Tellus, Ser. B Chem. Phys. Meteorol., 63(3), 340–351, doi:10.1111/j.1600-0889.2011.00531.x, 2011.

AMAP: AMAP assessment 2015: Black carbon and ozone as Arctic climate forcers, Arctic Monitoring and Assessment Programme (AMAP), Oslo, Norway., 2015.

Andreae, M. O. and Gelencsér, A.: Black carbon or brown carbon? The nature of light-absorbing carbonaceous aerosols, Atmos. Chem. Phys., 6(3), 3419–3463, doi:10.5194/acpd-6-3419-2006, 2006.

Bond, T. C., Streets, D. G., Yarber, K. F., Nelson, S. M., Woo, J. H. and Klimont, Z.: A technology-based global inventory of black and organic carbon emissions from combustion, J. Geophys. Res. D Atmos., 109(14), 1–43, doi:10.1029/2003JD003697, 2004.

Bond, T. C., Doherty, S. J., Fahey, D. W., Forster, P. M., Berntsen, T., Deangelo, B. J., Flanner, M. G., Ghan, S., Kärcher, B., Koch, D., Kinne, S., Kondo, Y., Quinn, P. K., Sarofim, M. C., Schultz, M. G., Schulz, M., Venkataraman, C., Zhang, H., Zhang, S., Bellouin, N., Guttikunda, S. K., Hopke, P. K., Jacobson, M. Z., Kaiser, J. W., Klimont, Z., Lohmann, U., Schwarz, J. P., Shindell, D., Storelvmo, T., Warren, S. G. and Zender, C. S.: Bounding the role of black carbon in the climate system: A scientific assessment, J. Geophys. Res. Atmos., 118(11), 5380–5552, doi:10.1002/jgrd.50171, 2013.

Brandt, R. E., Warren, S. G., Worby, A. P. and Grenfell, T. C.: Surface albedo of the Antarctic sea ice zone, J. Clim., 18(17), 3606–3622, doi:10.1175/JCLI3489.1, 2005.

Cavalli, F., Viana, M., Yttri, K. E., Genberg, J. and Putaud, J.-P.: Toward a standardised thermal-optical protocol for measuring atmospheric organic and elemental carbon: the EUSAAR protocol, Atmos. Meas. Tech., 3(1), 79–89, doi:10.5194/amt-3-79-2010, 2010.

620 Cavalli, F., Putaud, J.-P. and Yttri, K. E.: Availability and quality of the EC and OC
621 measurements within EMEP, including results of the fifth interlaboratory comparison of
622 analytical methods for carbonaceous particulate matter within EMEP (2012)., 2015.

623 Clarke, A. D. and Noone, K. J.: Soot in the arctic snowpack: a cause for perturbations in
624 radiative transfer, Atmos. Environ., 41(SUPPL.), 64–72, doi:10.1016/0004-6981(85)90113-1,
625 1985.

626 Doherty, S. J., Warren, S. G., Grenfell, T. C., Clarke, A. D. and Brandt, R. E.: Light-
627 absorbing impurities in Arctic snow, Atmos. Chem. Phys., 10(23), 11647–11680,
628 doi:10.5194/acp-10-11647-2010, 2010.

629 Doherty, S. J., Grenfell, T. C., Forsström, S., Hegg, D. L., Brandt, R. E. and Warren, S. G.:
630 Observed vertical redistribution of black carbon and other insoluble light-absorbing particles
631 in melting snow, J. Geophys. Res. Atmos., 118(11), 5553–5569, doi:10.1002/jgrd.50235,
632 2013.

633 Eckhardt, S., Cassiani, M., Evangeliou, N., Sollum, E., Pisso, I. and Stohl, A.: Source-
634 receptor matrix calculation for deposited mass with the Lagrangian particle dispersion model
635 FLEXPART v10.2 in backward mode, Geosci. Model Dev., 10, 4605–4618,
636 doi:10.5194/gmd-10-4605-2017, 2017.

637 Evangeliou, N., Balkanski, Y., Hao, W. M., Petkov, A., Silverstein, R. P., Corley, R.,
638 Nordgren, B. L., Urbanski, S. P., Eckhardt, S., Stohl, A., Tunved, P., Crepinsek, S., Jefferson,
639 A., Sharma, S., Nøjgaard, J. K. and Skov, H.: Wildfires in northern Eurasia affect the budget
640 of black carbon in the Arctic-a 12-year retrospective synopsis (2002-2013), Atmos. Chem.
641 Phys., 16(12), 7587–7604, doi:10.5194/acp-16-7587-2016, 2016.

642 Flanner, M. G., Zender, C. S., Randerson, J. T. and Rasch, P. J.: Present-day climate forcing
643 and response from black carbon in snow, J. Geophys. Res. Atmos., 112(11), 1–17,
644 doi:10.1029/2006JD008003, 2007.

645 Forsström, S., Isaksson, E., Skeie, R. B., Ström, J., Pedersen, C. A., Hudson, S. R., Berntsen,
646 T. K., Lihavainen, H., Godtliebsen, F. and Gerland, S.: Elemental carbon measurements in
647 European Arctic snow packs, J. Geophys. Res. Atmos., 118(24), 13614–13627,
648 doi:10.1002/2013JD019886, 2013.

649 Forster, C., Wandinger, U., Wotawa, G., James, P., Mattis, I., Althausen, D., Simmonds, P.,

O'Doherty, S., Jennings, S. G., Kleefeld, C., Schneider, J., Trickl, T., Kreipl, S., Jäger, H. and Stohl, A.: Transport of boreal forest fire emissions from Canada to Europe, J. Geophys. Res., 106, 22887, doi:10.1029/2001JD900115, 2001.

Giglio, L., Descloitres, J., Justice, C. O. and Kaufman, Y. J.: An enhanced contextual fire detection algorithm for MODIS, Remote Sens. Environ., 87(2–3), 273–282, doi:10.1016/S0034-4257(03)00184-6, 2003.

Giglio, L., Randerson, J. T. and van der Werf, G. R.: Analysis of daily, monthly, and annual burned area using the fourth-generation global fire emissions database (GFED4), J. Geophys. Res. Biogeosciences, 118, 317–328, doi:10.1002/jgrg.20042, 2013, 2013.

Grythe, H., Kristiansen, N. I., Groot Zwaaftink, C. D., Eckhardt, S., Ström, J., Tunved, P., Krejci, R. and Stohl, A.: A new aerosol wet removal scheme for the Lagrangian particle model FLEXPARTv10, Geosci. Model Dev., 10, 1447–1466, doi:10.5194/gmd-10-1447-2017, 2017.

Hadley, O. L., Corrigan, C. E., Kirchstetter, T. W., Cliff, S. S. and Ramanathan, V.: Measured black carbon deposition on the Sierra Nevada snow pack and implication for snow pack retreat, Atmos. Chem. Phys., 10(15), 7505–7513, doi:10.5194/acp-10-7505-2010, 2010.

Hansen, J. and Nazarenko, L.: Soot climate forcing via snow and ice albedos, Proc. Natl. Acad. Sci. U. S. A., 101(2), 423–428, doi:10.1073/pnas.2237157100, 2004.

Hao, W. M., Petkov, A., Nordgren, B. L., Silverstein, R. P., Corley, R. E., Urbanski, S. P., Evangeliou, N., Balkanski, Y. and Kinder, B.: Daily black carbon emissions from fires in Northern Eurasia from 2002 to 2013, Geosci. Model Dev. Discuss., (April), 1–24, doi:10.5194/gmd-2016-89, 2016.

Hegg, D. A., Warren, S. G., Grenfell, T. C., Doherty, S. J., Larson, T. V. and Clarke, A. D.: Source attribution of black carbon in arctic snow, Environ. Sci. Technol., 43(11), 4016–4021, doi:10.1021/es803623f, 2009.

Hegg, D. A., Warren, S. G., Grenfell, T. C., Doherty, S. J. and Clarke, A. D.: Sources of light-absorbing aerosol in arctic snow and their seasonal variation, Atmos. Chem. Phys., 10(22), 10923–10938, doi:10.5194/acp-10-10923-2010, 2010.

Hollingsworth, A., Engelen, R. J., Textor, C., Benedetti, A., Boucher, O., Chevallier, F.,

679 Dethof, A., Elbern, H., Eskes, H., Flemming, J., Granier, C., Kaiser, J. W., Morcrette, J. J.,
680 Rayner, P., Peuch, V. H., Rouil, L., Schultz, M. G. and Simmons, A. J.: Toward a monitoring
681 and forecasting system for atmospheric composition: The GEMS project, Bull. Am. Meteorol.
682 Soc., 89(8), 1147–1164, doi:10.1175/2008BAMS2355.1, 2008.

683 Huang, K. and Fu, J. S.: Data Descriptor : A global gas flaring black carbon emission rate
684 dataset from 1994 to 2012, Nature, 1–11, doi:10.1038/sdata.2016.104, 2016.

685 Huang, K., Fu, J. S., Hodson, E. L., Dong, X., Cresko, J., Prikhodko, V. Y., Storey, J. M. and
686 Cheng, M. D.: Identification of missing anthropogenic emission sources in Russia:
687 Implication for modeling arctic haze, Aerosol Air Qual. Res., 14(7), 1799–1811,
688 doi:10.4209/aaqr.2014.08.0165, 2014.

689 Ingvander, S., Rosqvist, G., Svensson, J. and Dahlke, H. E.: Seasonal and interannual
690 variability of elemental carbon in the snowpack of Storglaci??ren, northern Sweden, Ann.
691 Glaciol., 54(62), 50–58, doi:10.3189/2013AoG62A229, 2013.

692 Jankowski, N., Schmidl, C., Marr, I. L., Bauer, H. and Puxbaum, H.: Comparison of methods
693 for the quantification of carbonate carbon in atmospheric PM10 aerosol samples, Atmos.
694 Environ., 42(34), 8055–8064, doi:10.1016/j.atmosenv.2008.06.012, 2008.

695 Klimont, Z., Kupiainen, K., Heyes, C., Purohit, P., Cofala, J., Rafaj, P., Borken-Kleefeld, J.
696 and Schöpp, W.: Global anthropogenic emissions of particulate matter including black
697 carbon, Atmos. Chem. Phys. Discuss., (October), 1–72, doi:10.5194/acp-2016-880, 2016.

698 Lamarque, J. F., Shindell, D. T., Josse, B., Young, P. J., Cionni, I., Eyring, V., Bergmann, D.,
699 Cameron-Smith, P., Collins, W. J., Doherty, R., Dalsoren, S., Faluvegi, G., Folberth, G.,
700 Ghan, S. J., Horowitz, L. W., Lee, Y. H., MacKenzie, I. A., Nagashima, T., Naik, V.,
701 Plummer, D., Righi, M., Rumbold, S. T., Schulz, M., Skeie, R. B., Stevenson, D. S., Strode,
702 S., Sudo, K., Szopa, S., Voulgarakis, A. and Zeng, G.: The atmospheric chemistry and climate
703 model intercomparison Project (ACCMIP): Overview and description of models, simulations
704 and climate diagnostics, Geosci. Model Dev., 6(1), 179–206, doi:10.5194/gmd-6-179-2013,
705 2013.

706 Law, K. S. and Stohl, A.: Arctic Air Pollution: Origins and Impacts, Science (80-.).,
707 315(5818), 1537–1540, doi:10.1126/science.1137695, 2007.

708 Lelieveld, J., Evans, J. S., Fnais, M., Giannadaki, D. and Pozzer, A.: The contribution of

709 outdoor air pollution sources to premature mortality on a global scale., Nature, 525(7569),
710 367–71, doi:10.1038/nature15371, 2015.

711 Liu, J., Fan, S., Horowitz, L. W. and Levy, H.: Evaluation of factors controlling long-range
712 transport of black carbon to the Arctic, J. Geophys. Res., 116(D4), D04307,
713 doi:10.1029/2010JD015145, 2011.

714 Macdonald, K. M., Sharma, S., Toom, D., Chivulescu, A., Hanna, S., Bertram, A., Platt, A.,
715 Elsasser, M., Huang, L., Chellman, N., McConnell, J. R., Bozem, H., Kunkel, D., Lei, Y. D.,
716 Evans, G. J. and Abbatt, J. P. D.: Observations of Atmospheric Chemical Deposition to High
717 Arctic Snow, Atmos. Chem. Phys., 17, 5775–5788, doi:10.5194/acp-17-5775-2017, 2017.

718 McConnell, J. R., Edwards, R., Kok, G. L., Flanner, M. G., Zender, C. S., Saltzman, E. S.,
719 Banta, J. R., Pasteris, D. R., Carter, M. M. and Kahl, J. D. W.: 20th-Century Industrial Black
720 Carbon Emissions Altered Arctic Climate Forcing, Science (80-.)., 317(5843), 1381–1384,
721 doi:10.1126/science.1144856, 2007.

722 Ogren, J. A., Charlson, R. J. and Groblicki, P. J.: Determination of elemental carbon in
723 rainwater, Anal. Chem., 55(9), 1569–1572, doi:10.1021/ac00260a027, 1983.

724 Olivier, J. G. J., Aardenne, J. A. Van, Dentener, F. J., Pagliari, V., Ganzeveld, L. N. and
725 Peters, J. A. H. W.: Recent trends in global greenhouse gas emissions:regional trends 1970–
726 2000 and spatial distributionof key sources in 2000, Environ. Sci., 2(2–3), 81–99,
727 doi:10.1080/15693430500400345, 2005.

728 Petzold, A., Ogren, J. A., Fiebig, M., Laj, P., Li, S. M., Baltensperger, U., Holzer-Popp, T.,
729 Kinne, S., Pappalardo, G., Sugimoto, N., Wehrli, C., Wiedensohler, A. and Zhang, X. Y.:
730 Recommendations for reporting black carbon measurements, Atmos. Chem. Phys., 13(16),
731 8365–8379, doi:10.5194/acp-13-8365-2013, 2013.

732 Popovicheva, O. B., Evangeliou, N., Eleftheriadis, K., Kalogridis, A. C., Movchan, V.,
733 Sitnikov, N., Eckhardt, S., Makshtas, A. and Stohl, A.: Black carbon sources constrained by
734 observations and modeling in the Russian high Arctic, Environ. Sci. Technol., submitted,
735 doi:10.1021/acs.est.6b05832, 2017.

736 Qi, L., Li, Q., Henze, D. K., Tseng, H.-L. and He, C.: Sources of Springtime Surface Black
737 Carbon in the Arctic: An Adjoint Analysis, Atmos. Chem. Phys. Discuss., (February), 1–32,
738 doi:10.5194/acp-2016-1112, 2017.

739 Ruppel, M. M., Isaksson, I., Ström, J., Beaudon, E., Svensson, J., Pedersen, C. A. and
740 Korhola, A.: Increase in elemental carbon values between 1970 and 2004 observed in a 300-
741 year ice core from Holtedahlfonna (Svalbard), Atmos. Chem. Phys., 14(20), 11447–11460,
742 doi:10.5194/acp-14-11447-2014, 2014.

743 Sand, M., Berntsen, T. K., von Salzen, K., Flanner, M. G., Langner, J. and Victor, D. G.:
744 Response of Arctic temperature to changes in emissions of short-lived climate forcers, Nat.
745 Clim. Chang., 6(November), 1–5, doi:10.1038/nclimate2880, 2015.

746 Seibert, P. and Frank, A.: Source-receptor matrix calculation with a Lagrangian particle
747 dispersion model in backward mode, Atmos. Chem. Phys., 4(1), 51–63, doi:10.5194/acp-4-
748 51-2004, 2004.

749 Sharma, S., Ishizawa, M., Chan, D., Lavoué, D., Andrews, E., Eleftheriadis, K. and
750 Maksyutov, S.: 16-year simulation of arctic black carbon: Transport, source contribution, and
751 sensitivity analysis on deposition, J. Geophys. Res. Atmos., 118(2), 943–964,
752 doi:10.1029/2012JD017774, 2013.

753 Shiraiwa, M., Kondo, Y., Moteki, N., Takegawa, N., Sahu, L. K., Takami, A., Hatakeyama,
754 S., Yonemura, S. and Blake, D. R.: Radiative impact of mixing state of black carbon aerosol
755 in Asian outflow, J. Geophys. Res. Atmos., 113(24), 1–13, doi:10.1029/2008JD010546, 2008.

756 Singh, P. and Haritashya, U. K.: Encyclopedia of Snow, Ice and Glaciers., 2011.

757 Slinn, W. G. N.: Predictions for particle deposition to vegetative canopies, Atmos. Environ.,
758 16, 1785–1794, doi:10.1016/0004-6981(82)90271-2, 1982.

759 Stein, O., Flemming, J., Inness, A., Kaiser, J. W. and Schultz, M. G.: Global reactive gases
760 forecasts and reanalysis in the MACC project, J. Integr. Environ. Sci., 8168(October 2014),
761 1–14, doi:10.1080/1943815X.2012.696545, 2012.

762 Stohl, A., Hittenberger, M. and Wotawa, G.: Validation of the lagrangian particle dispersion
763 model FLEXPART against large-scale tracer experiment data, Atmos. Environ., 32(24),
764 4245–4264, doi:10.1016/S1352-2310(98)00184-8, 1998.

765 Stohl, A., Forster, C., Eckhardt, S., Spichtinger, N., Huntrieser, H., Heland, J., Schlager, H.,
766 Wilhelm, S., Arnold, F. and Cooper, O.: A backward modeling study of intercontinental
767 pollution transport using aircraft measurements, J. Geophys. Res. Atmos., 108(D12), 4370,

768 doi:10.1029/2002JD002862, 2003.

769 Stohl, A., Forster, C., Frank, A., Seibert, P. and Wotawa, G.: Technical note: The Lagrangian
770 particle dispersion model FLEXPART version 6.2, Atmos. Chem. Phys., 5(9), 2461–2474,
771 doi:10.5194/acp-5-2461-2005, 2005.

772 Stohl, A., Andrews, E., Burkhart, J. F., Forster, C., Herber, A., Hoch, S. W., Kowal, D.,
773 Lunder, C., Mefford, T., Ogren, J. A., Sharma, S., Spichtinger, N., Stebel, K., Stone, R.,
774 Ström, J., Tørseth, K., Wehrli, C. and Yttri, K. E.: Pan-Arctic enhancements of light
775 absorbing aerosol concentrations due to North American boreal forest fires during summer
776 2004, J. Geophys. Res. Atmos., 111(22), 1–20, doi:10.1029/2006JD007216, 2006.

777 Stohl, A., Klimont, Z., Eckhardt, S., Kupiainen, K., Shevchenko, V. P., Kopeikin, V. M. and
778 Novigatsky, A. N.: Black carbon in the Arctic: The underestimated role of gas flaring and
779 residential combustion emissions, Atmos. Chem. Phys., 13(17), 8833–8855, doi:10.5194/acp-
780 13-8833-2013, 2013.

781 Stohl, A., Aamaas, B., Amann, M., Baker, L. H., Bellouin, N., Berntsen, T. K., Boucher, O.,
782 Cherian, R., Collins, W., Daskalakis, N., Dusinska, M., Eckhardt, S., Fuglestvedt, J. S., Harju,
783 M., Heyes, C., Hodnebrog, Hao, J., Im, U., Kanakidou, M., Klimont, Z., Kupiainen, K., Law,
784 K. S., Lund, M. T., Maas, R., MacIntosh, C. R., Myhre, G., Myriokefalitakis, S., Olivié, D.,
785 Quaas, J., Quennehen, B., Raut, J. C., Rumbold, S. T., Samset, B. H., Schulz, M., Seland,
786 Shine, K. P., Skeie, R. B., Wang, S., Yttri, K. E. and Zhu, T.: Evaluating the climate and air
787 quality impacts of short-lived pollutants, Atmos. Chem. Phys., 15(18), 10529–10566,
788 doi:10.5194/acp-15-10529-2015, 2015.

789 Svensson, J., Ström, J., Hansson, M., Lihavainen, H. and Kerminen, V.-M.: Observed metre
790 scale horizontal variability of elemental carbon in surface snow, Environ. Res. Lett., 8(3),
791 34012, doi:10.1088/1748-9326/8/3/034012, 2013.

792 Turner, M. D., Henze, D. K., Capps, S. L., Hakami, A., Zhao, S., Resler, J., Carmichael, G.
793 R., Stanier, C. O., Baek, J., Sandu, A., Russell, A. G., Nenes, A., Pinder, R. W., Napelenok, S.
794 L., Bash, J. O., Percell, P. B. and Chai, T.: Premature deaths attributed to source-specific BC
795 emissions in six urban US regions, , 10(114014), doi:10.1088/1748-9326/10/11/114014/meta,
796 2005.

797 Wang, Q., Jacob, D. J., Fisher, J. A., Mao, J., Leibensperger, E. M., Carouge, C. C., Le Sager,

798 P., Kondo, Y., Jimenez, J. L., Cubison, M. J. and Doherty, S. J.: Sources of carbonaceous
799 aerosols and deposited black carbon in the Arctic in winter-spring: Implications for radiative
800 forcing, Atmos. Chem. Phys., 11(23), 12453–12473, doi:10.5194/acp-11-12453-2011, 2011.

801 Warren, S. G. and Wiscombe, W. J.: A Model for the Spectral Albedo of Snow. II: Snow
802 Containing Atmospheric Aerosols, J. Atmos. Sci., 37, 2734–2745, doi:10.1175/1520-
803 0469(1980)037<2734:AMFTSA>2.0.CO;2, 1980.

804 Winiger, P., Andersson, A., Eckhardt, S., Stohl, A., Semiletov, I. P., Dudarev, O. V., Charkin,
805 A., Shakhova, N., Klimont, Z., Heyes, C. and Gustafsson, Ö.: Siberian Arctic black carbon
806 sources constrained by model and observation, Proc. Natl. Acad. Sci., 1–8,
807 doi:10.1073/pnas.1613401114, 2017.

808

FIGURE CAPTIONS FOR MANUSCRIPT

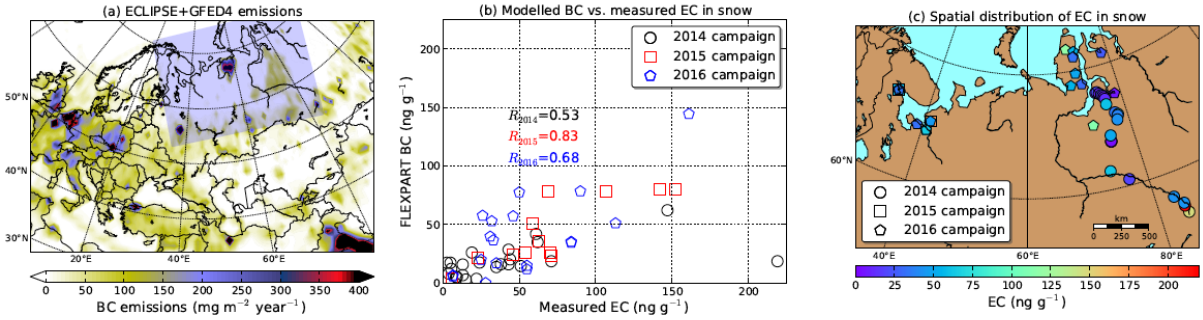

Figure 1. (a) Total emissions of BC (anthropogenic emissions from ECLIPSE (Klimont et al., 2016) and biomass burning from GFED4 (Giglio et al., 2013). The blue shade shows the area of interest that is zoomed on the right. (b) Comparison of modelled BC concentrations in snow with measured EC concentrations. (c) Spatial distribution of EC in snow measured by thermal optical analysis (TOA) of filtered snow samples from northwestern European Russia and Western Siberia in spring–time 2014, 2015 and 2016.

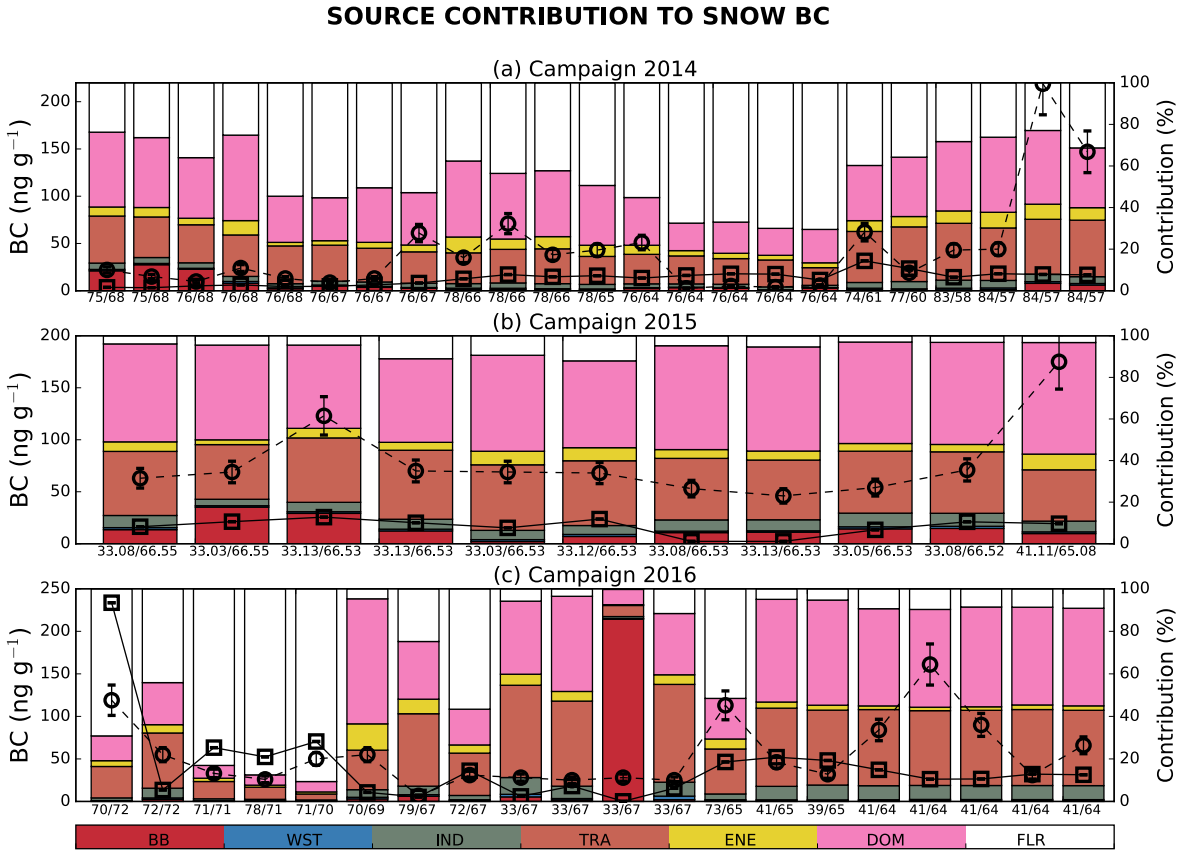

Figure 2. Contribution from the various emission categories considered in the ECLIPSE and GFED inventories to simulated BC concentrations in snow in (a) 2014, (b) 2015 and (c) 2016 in Western Siberia and northwestern European Russia. BB stands for biomass burning, WST for waste burning, IND for industrial combustion and processing, TRA for surface transportation, ENE for emissions from energy conversion, and extraction, DOM for residential and commercial combustion, and FLR for gas flaring. Bars show the relative source contribution (0 –100%, right axis) and are sorted, from left to right, from the northernmost to the southernmost measurement location (coordinates are reported on the bottom as longitude/latitude). Measured EC concentrations in snow are reported with open circles, whereas modelled BC is shown with open rectangles (left axis).

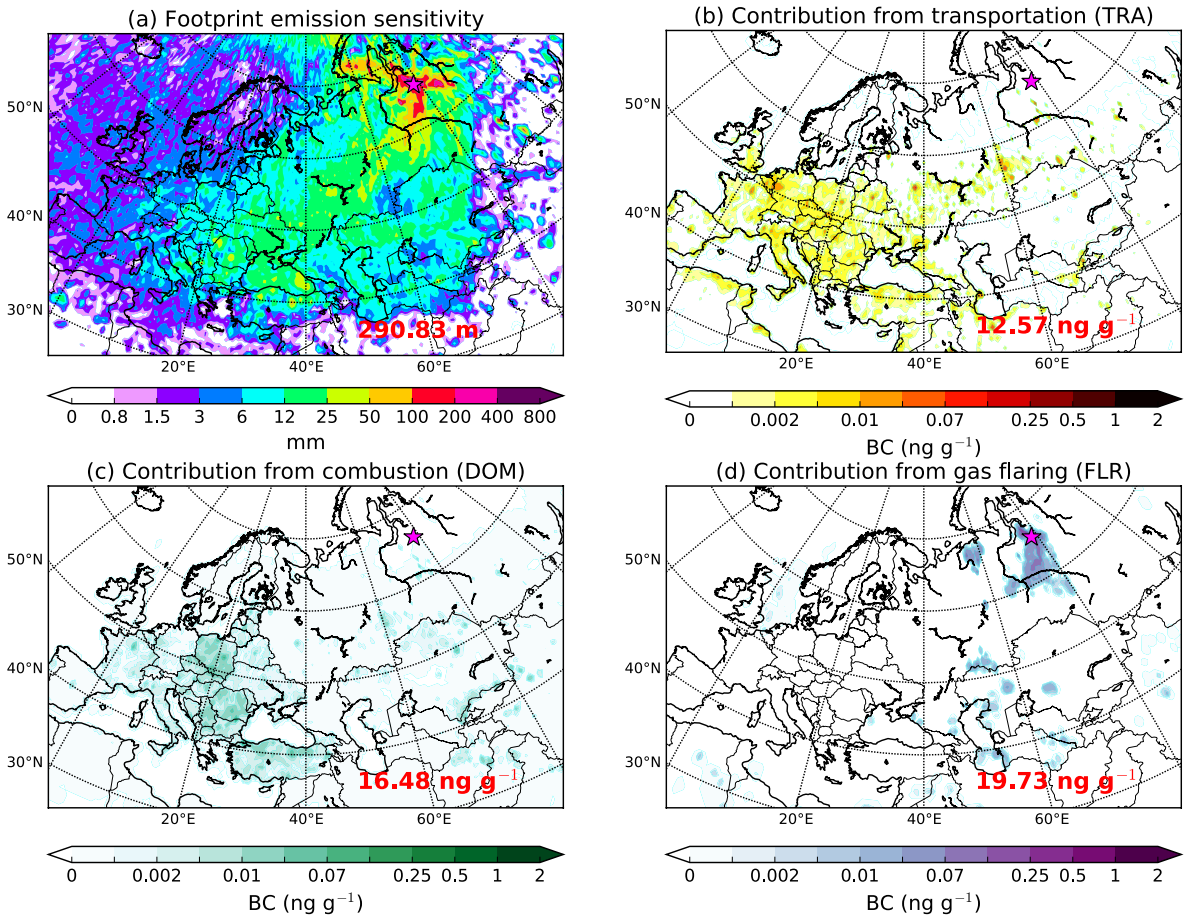

830

831 **Figure 3.** (a) FLEXPART emission sensitivity, contribution from (b) transportation (TRA),
832 (c) residential and commercial combustion (DOM) and (d) gas flaring (FLR) to the maximum
833 measured concentration of snow EC recorded along the transect from Tomsk to Yamal
834 Peninsula in Western Siberia during the campaign of 2014.

835

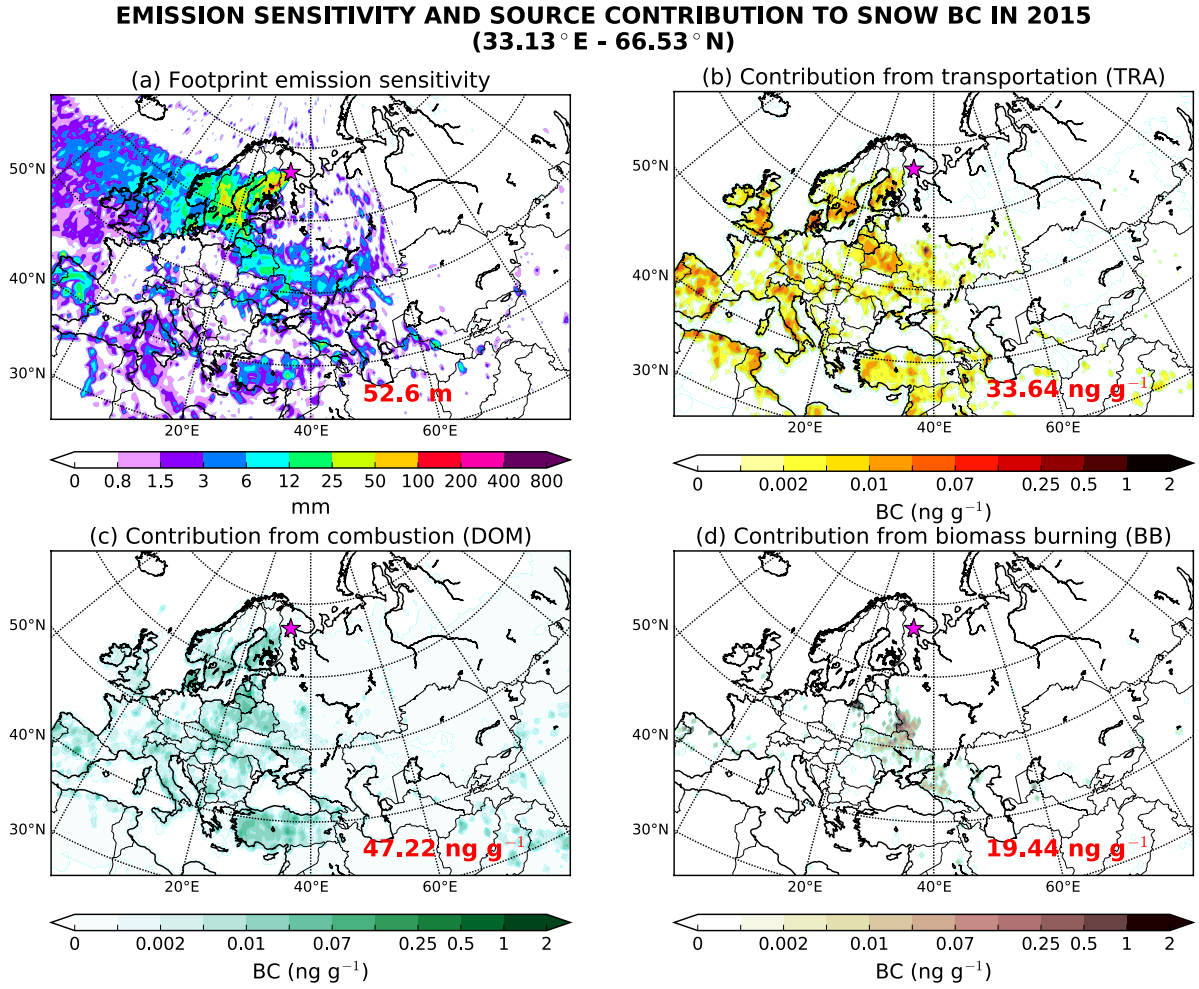

836

837 **Figure 4.** (a) FLEXPART emission sensitivity, (b) contribution from transportation (TRA),
838 (c) residential and commercial combustion (DOM) and (d) gas flaring (FLR) to the maximum
839 measured concentration of snow EC recorded in northwestern European Russia (Kindo
840 Peninsula and Arkhangelsk region) during the campaign of 2015.

841

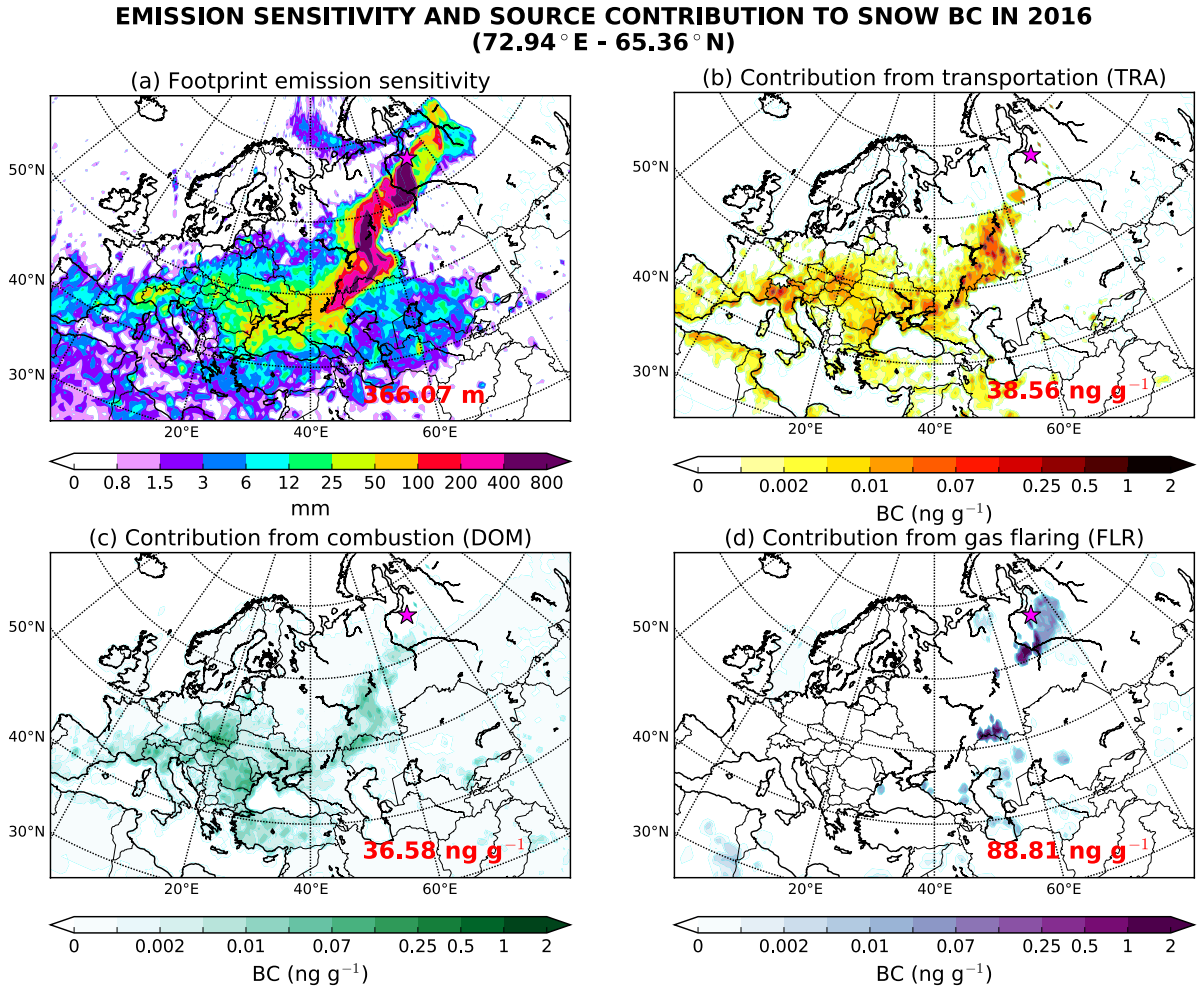

842

843 **Figure 5.** (a) FLEXPART emission sensitivity and (b) contribution from transportation
844 (TRA), (c) residential and commercial combustion (DOM) and (d) gas flaring (FLR) to the
845 maximum measured concentration of snow EC recorded in Kindo Peninsula, Arkhangelsk and
846 Yamal Peninsula (northwestern European Russia, Western Siberia) during the campaign of
847 2016.

848

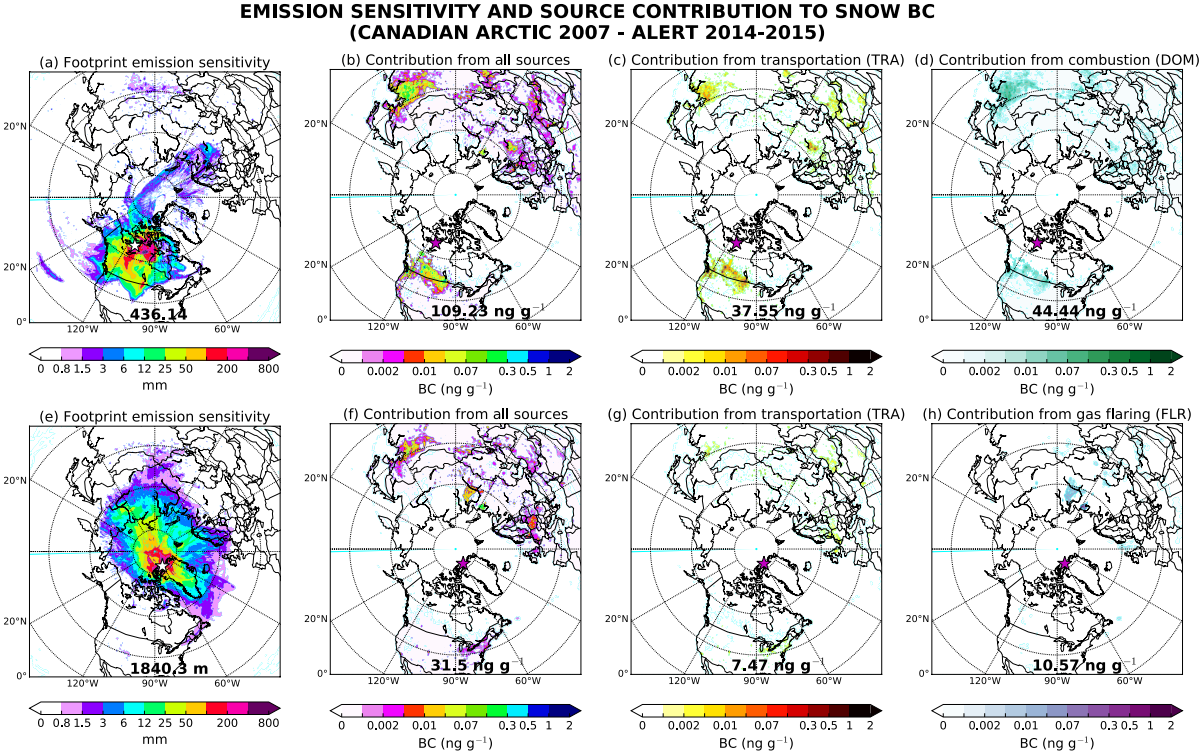

849

850 **Figure 6.** (a–d) Footprint emission sensitivity and major contribution from all sources, TRA
851 and DOM averaged for the samples that showed overestimated modelled concentrations of
852 BC in 2007 (Doherty et al., 2010). (e–h) Footprint emission sensitivity and contribution from
853 all sources, TRA and FLR for the samples collected in Alert (Macdonald et al., 2017) that
854 model overestimated by more than three times.

855

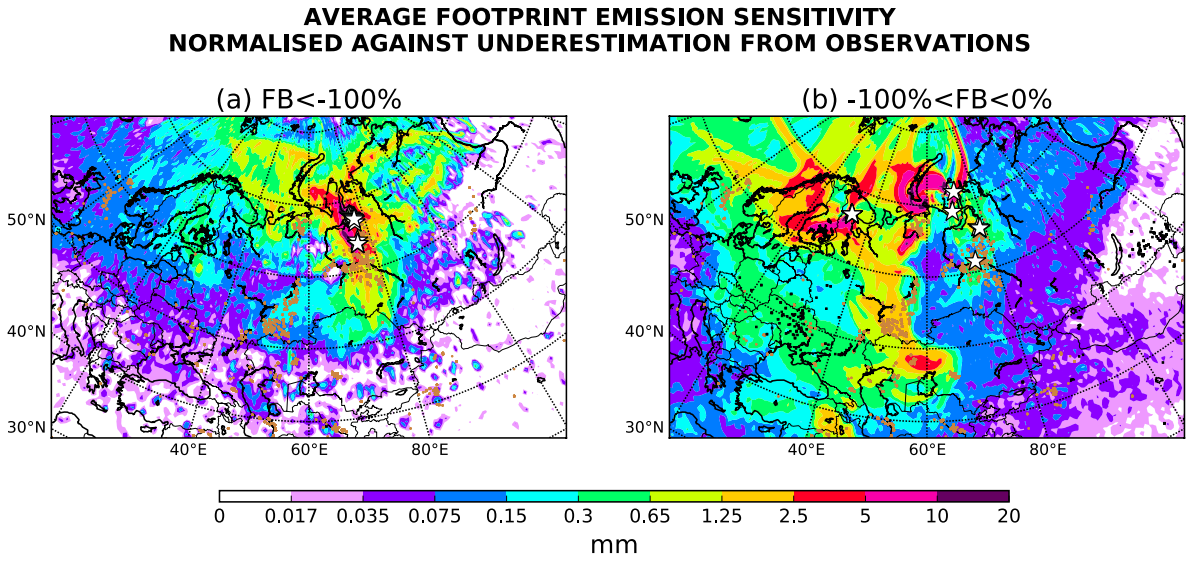

856

857 **Figure 7.** (a) Footprint emission sensitivity from FLEXPART averaged for the sampling
858 points where the model underestimated observations significantly ($\boldsymbol{FB < -100\%}$) and (b)
859 less significantly ($\boldsymbol{-100\% < FB < 0\%}$). Black squares show the locations of active fires
860 detected by MODIS (Moderate Resolution Imaging Spectroradiometer) (Giglio et al., 2003).
861 Brown dots show the location of gas flaring sites from the Global Gas Flaring Reduction
862 Partnership (GGFR) (http://www.worldbank.org/en/programs/gasflaringreduction).

863

FIGURE & TABLE CAPTIONS FOR SUPPLEMENTS

Figure S 1. Fractional bias ($\boldsymbol{FB = [(C_m - C_o)/(C_m + C_o)\times 0.5]\times 100\%}$) for all samples collected from the three campaigns in Western Siberia and northwestern European Russia in 2014, 2015 and 2016. MFB (mean fractional bias) is the fractional bias averaged for all snow samples from 2014, 2015 and 2016, whereas RMSE is the root mean square error in ng g^{-1}).

Figure S 2. (a) Distribution of snow measurements of BC adopted from Doherty et al. (2010) in the Arctic from 2005 to 2009. (b) Simulated (FLEXPART) BC concentrations in snow for the same period (right). MFB, RMSE and correlation coefficient (R) values are further given.

Figure S 3. Timeseries of simulated and measured BC concentrations in snow collected in Alert (Macdonald et al., 2017). Correlation coefficient (R) between modelled and measured BC, RMSE and MFB values are also shown.

Figure S 4. (a) Average footprint emission sensitivity and (b–f) source contribution (from all sources, TRA, DOM, FLR and BB) for all the samples located in northwestern European Russia.

Figure S 5. (a) Average footprint emission sensitivity and (b–f) source contribution (from all sources, TRA, DOM, FLR and BB) for all the samples located in Western Siberia (north of 62 °N).

Figure S 6. (a) Average footprint emission sensitivity and (b–f) source contribution (from all sources, TRA, DOM, FLR and BB) for all the samples located in Western Siberia (south of 62 °N).

Table S 1. Information about the samples collected in springtime of 2014, 2015 and 2016 in Western Russia.

Table S 2. $\boldsymbol{EC^{corr}_{CO_3^{2-}}}$ to $\boldsymbol{EC}$ ratio (Mean ± SD; Min - Max), showing overestimation of $\boldsymbol{EC}$ due to $\boldsymbol{EC_{CO_3^{2-}}}$ in the filtered snow samples.